Northumbria
University
NEWCASTLE

Static and vibration analysis of isotropic and functionally graded sandwich plates using an edge-based MITC3 finite elements

Trung-Kien Nguyen[a,*], Van-Hau Nguyen[a], Thanh Chau-Dinh[a], Thuc P. Vo[b,*], Xuan-Hung Nguyen[c]

[a]*Faculty of Civil Engineering and Applied Mechanics, HCMC University of Technology and Education, 1 Vo Van Ngan Street, Thu Duc District, Ho Chi Minh City, Viet Nam*
[b]*Faculty of Engineering and Environment, Northumbria University, Newcastle upon Tyne, NE1 8ST, UK.*
[c]*CIRTech, HUTECH University, 475A Dien Bien Phu Street, Binh Thanh District, Ho Chi Minh City, Viet Nam*

Abstract

Static and vibration analysis of isotropic and functionally graded sandwich plates using a higher-order shear deformation theory is presented in this paper. Lagrangian functional is used to derive the equations of motion. The mixed interpolation of tensorial components (MITC) approach and edge-based-strain technique is used to solve problems. A MITC3 three-node triangle element with 7 degree-of-freedoms per nodes that only requires the C^0-type continuity is developed. Numerical results for isotropic and functionally graded sandwich plates with different boundary conditions are proposed to validate the developed theory and to investigate effects of material distribution, side-to-thickness ratio, thickness ratio of layers and boundary conditions on the deflection, stresses and natural frequencies of the plates.

Keywords: Functionally graded sandwich plates; Static; Vibration; Smooth finite element method; MITC3.

1. Introduction

Functionally graded material (FGM) is an advanced composite material whose constituent volume fractions vary smoothly according to a required performance, the isotropic and functionally graded (FG) structures therefore avoid material discontinuity found in conventional laminated composites. This structural material is suitable for various applications in the engineering fields. Large applications of FGMs have led to the development of different theories to predict accurately their responses. In order to account shear deformation effect of FG plates, it is known that the first-shear deformation theory (FSDT) ([1–10]) is the simplest one, however it requires an appropriate shear correction factor to correct free-traction boundary condition of shear stresses. The higher-order shear deformation theories

*Corresponding author, tel.: +848 3897 2092
Email addresses: kiennt@hcmute.edu.vn (Trung-Kien Nguyen), thuc.vo@northumbria.ac.uk (Thuc P. Vo)

(HSDTs) with higher-order variation of the in-plane displacements (HSDT) ([6, 11–24]), or both in-plane and out-of-plane displacements (Quasi-3D) ([25–36]) require no shear correction. In order to overcome interface problems between faces and core found in conventional sandwich structures, FG sandwich plates have recently been used. Consequently, static, vibration and buckling behaviours of these plates have been attracted the authors with analytical and numerical approaches ([6, 22, 24, 37–52]). Due to the limitation of analytical solutions in practical applications, numerical methods have been developed with various degrees of success. Among them, the finite element method (FEM) is the most popular one. Different approaches have been studied to overcome the stiffness excess phenomena characterizing the shear-locking problem, among which the mixed interpolation of tensorial components (MITC) approach has been recently used as a very successful locking removal technique for plate and shell finite elements ([53–57]. In fact, the MITC4-quadrilateral shell finite elements were first developed by Dvorkin and Bathe [54], then MITC9- and MITC16-quadrilateral shell finite elements by Bucalem and Bathe [55], MITC3- and MITC6-isotropic triangular shell elements by Lee and Bathe [53, 58]. Based on a strain smoothing technique, Liu et al. [59] also developed a family of smoothed finite element methods (SFEM) that can be categorized in the following types: cell-based smoothing (CS-FEM) [60], node-based smoothing (NS-FEM) [61], edge-based smoothing (ES-FEM) [62], and face-based smoothing (FS-FEM) [63].

The objective of this paper is to present static and vibration analysis of isotropic and FG sandwich plates. It is based on a higher-order shear deformation theory which accounts a higher-order variation of transverse shear stresses. A MITC3 three-node triangle element with 7 degree-of-freedoms per nodes that only requires the C^0-type continuity is used, and then an edge-based strain smoothing technique is considered. Numerical results for isotropic and functionally graded sandwich plates with different boundary conditions are proposed to validate the developed theory and to investigate effects of material distribution, side-to-thickness ratio, thickness ratio of layers and boundary conditions on the deflection, stresses and natural frequencies of the plates.

2. Theoretical formulation

2.1. Isotropic and functionally graded plates

Consider a FG plate under a transverse mechanical load at the top surface with the bounded domain Ω and uniform thickness h as Fig. 1. The material properties such as Young's modulus E, density ρ and Poisson's ratio ν are assumed to vary continuously through the thickness. Three types of FG plates are considered.

2.1.1. Type A: isotropic FG plates

The plate is graded from metal to ceramic with the volume fraction of ceramic material V_c is given (Fig. 1a):

$$V_c(z) = \left(\frac{2z+h}{2h}\right)^p \tag{1}$$

where p is the power-law index, which is positive and $z \in [-\frac{h}{2}, \frac{h}{2}]$.

2.1.2. Type B: sandwich plates with FG core

The top and bottom face is made of ceramic and metal, while the core is graded from metal to ceramic (Fig. 1b). The volume fraction function of ceramic material of the jth layer $V_c^{(j)}$ is defined by:

$$\begin{cases} V_c^{(1)}(z) = 0 & \text{for} \quad z \in [h_0, h_1] \\ V_c^{(2)}(z) = \left(\frac{z-h_1}{h_2-h_1}\right)^p & \text{for} \quad z \in [h_1, h_2] \\ V_c^{(3)}(z) = 1 & \text{for} \quad z \in [h_2, h_3] \end{cases} \tag{2}$$

2.1.3. Type C: sandwich plates with FG faces

The top and bottom face is graded from metal to ceramic, while to core is ceramic (Fig. 1c). The volume fraction function of ceramic material of the jth layer $V_c^{(j)}$ is defined by:

$$\begin{cases} V_c^{(1)}(z) = \left(\frac{z-h_0}{h_1-h_0}\right)^p & \text{for} \quad z \in [h_0, h_1] \\ V_c^{(2)}(z) = 1 & \text{for} \quad z \in [h_1, h_2] \\ V_c^{(3)}(z) = \left(\frac{z-h_3}{h_2-h_3}\right)^p & \text{for} \quad z \in [h_2, h_3] \end{cases} \tag{3}$$

The effective material properties (E, ν, ρ) at the jth layer of FG plates are calculated by using the rule of mixture:

$$P^{(j)}(z) = (P_c - P_m)V_c^{(j)}(z) + P_m \tag{4}$$

where P_m and P_c are the material properties of metal and ceramic.

2.2. Kinematics, strains and stresses

It is known that the HSDTs neglect the thickness stretching effect(normal deformation ϵ_{zz}=0), which causes the independent transverse displacement through the plate

thickness. As introduced by Koiter [64], the magnitude of thickness stretching plays the same role as the shear deformation effect. In order to consider thickness stretching effect, Carrera et al. [65] introduced a Carrera Unified Formulation(CUF). This formulation has been applied to anlyse FG plates by Carrera and his colleagues [27, 28, 37, 39, 66]. In practice, although the higher-order variation of both in-plane and out-of-plane displacements predicts generally more accurate than the HSDTs, it appears to be complicated for implementation and costs due to the increase of variables. The displacement field of the present study based on a C^0-HSDT model is given by ([67]):

$$\begin{aligned} u_1(x,y,z) &= u(x,y) + \left(z + cz^3\right)\theta_x(x,y) + cz^3\phi_x(x,y) \\ u_2(x,y,z) &= v(x,y) + \left(z + cz^3\right)\theta_y(x,y) + cz^3\phi_y(x,y) \\ u_3(x,y,z) &= w(x,y) \end{aligned} \tag{5}$$

where u, v, w, θ_x, θ_y, ϕ_x and ϕ_y are seven unknown mid-surface displacements of the plate, $c = -\frac{4}{3h^2}$.

The compact form of strain field is expressed by:

$$\boldsymbol{\epsilon} = \boldsymbol{\epsilon}^{(0)} + z\boldsymbol{\epsilon}^{(1)} + z^3\boldsymbol{\epsilon}^{(2)} \tag{6a}$$

$$\boldsymbol{\gamma}^s = \boldsymbol{\gamma}^{(0)} + z^2\boldsymbol{\gamma}^{(1)} \tag{6b}$$

where

$$\boldsymbol{\epsilon}^{(0)} = \left\{ \begin{array}{c} \epsilon_{xx}^{(0)} \\ \epsilon_{yy}^{(0)} \\ \gamma_{xy}^{(0)} \end{array} \right\} = \left\{ \begin{array}{c} u_{,x} \\ v_{,y} \\ u_{,y} + v_{,x} \end{array} \right\}, \tag{7a}$$

$$\boldsymbol{\epsilon}^{(1)} = \left\{ \begin{array}{c} \epsilon_{xx}^{(1)} \\ \epsilon_{yy}^{(1)} \\ \gamma_{xy}^{(1)} \end{array} \right\} = \left\{ \begin{array}{c} \theta_{x,x} \\ \theta_{y,y} \\ \theta_{x,y} + \theta_{y,x} \end{array} \right\}, \tag{7b}$$

$$\boldsymbol{\epsilon}^{(2)} = \left\{ \begin{array}{c} \epsilon_{xx}^{(2)} \\ \epsilon_{yy}^{(2)} \\ \gamma_{xy}^{(2)} \end{array} \right\} = c\left\{ \begin{array}{c} \theta_{x,x} + \phi_{x,x} \\ \theta_{y,y} + \phi_{y,y} \\ \theta_{x,y} + \theta_{y,x} + \phi_{x,y} + \phi_{y,x} \end{array} \right\}, \tag{7c}$$

$$\boldsymbol{\gamma}^{(0)} = \left\{ \begin{array}{c} \gamma_{xz}^{(0)} \\ \gamma_{yz}^{(1)} \end{array} \right\} = \left\{ \begin{array}{c} \theta_x + w_{,x} \\ \theta_y + w_{,y} \end{array} \right\}, \boldsymbol{\gamma}^{(1)} = \left\{ \begin{array}{c} \gamma_{xz}^{(1)} \\ \gamma_{yz}^{(1)} \end{array} \right\} = 3c\left\{ \begin{array}{c} \theta_x + \phi_x \\ \theta_y + \phi_y \end{array} \right\} \tag{7d}$$

where the comma indicates partial differentiation with respect to the coordinate subscript that follows.

The linear stress-strain relations are given by:

$$\left\{ \begin{array}{c} \sigma_{xx} \\ \sigma_{yy} \\ \sigma_{xy} \end{array} \right\} = \left[\begin{array}{ccc} C_{11} & C_{12} & 0 \\ C_{12} & C_{22} & 0 \\ 0 & 0 & C_{66} \end{array} \right] \left\{ \begin{array}{c} \epsilon_{xx} \\ \epsilon_{yy} \\ \gamma_{xy} \end{array} \right\} \tag{8a}$$

$$\left\{ \begin{array}{c} \sigma_{xz} \\ \sigma_{yz} \end{array} \right\} = \left[\begin{array}{cc} C_{55} & 0 \\ 0 & C_{44} \end{array} \right] \left\{ \begin{array}{c} \gamma_{xz} \\ \gamma_{yz} \end{array} \right\} \tag{8b}$$

where

$$C_{11}(z) = C_{22}(z) = \frac{E(z)}{1-\nu(z)^2}, C_{12}(z) = \nu(z) C_{11}(z) \tag{9a}$$

$$C_{44}(z) = C_{55}(z) = C_{66}(z) = \frac{E(z)}{2(1+\nu(z))} \tag{9b}$$

Eqs. (8a) and (8b) can be rewritten under compact form:

$$\boldsymbol{\sigma} = \mathbf{C}\boldsymbol{\epsilon} \tag{10a}$$

$$\boldsymbol{\sigma}^s = \mathbf{C}^s \boldsymbol{\gamma}^s \tag{10b}$$

2.3. Energy principle

Lagrangian functional is used to derive the equations of motion:

$$\Pi = \mathcal{U} + \mathcal{V} - \mathcal{K} \tag{11}$$

where $\mathcal{U}$, $\mathcal{V}$ and $\mathcal{K}$ denote the strain energy, work done, and kinetic energy of the plate, respectively. The strain energy is given by:

$$\mathcal{U} = \frac{1}{2} \int_A \left(\boldsymbol{\epsilon}_p^T \mathbf{D}^* \boldsymbol{\epsilon}_p + \boldsymbol{\epsilon}_s^T \mathbf{D}_s^* \boldsymbol{\epsilon}_s \right) \mathrm{d}A \tag{12}$$

where $\boldsymbol{\epsilon}_p^T = [\boldsymbol{\epsilon}^{(0)} \quad \boldsymbol{\epsilon}^{(1)} \quad \boldsymbol{\epsilon}^{(2)}]$, $\boldsymbol{\epsilon}_s^T = [\boldsymbol{\gamma}^{(0)} \quad \boldsymbol{\gamma}^{(1)}]$,

$$\mathbf{D}^* = \left[\begin{array}{ccc} \mathbf{A} & \mathbf{B} & \mathbf{E} \\ \mathbf{B} & \mathbf{D} & \mathbf{F} \\ \mathbf{E} & \mathbf{F} & \mathbf{H} \end{array} \right], \mathbf{D}_s^* = \left[\begin{array}{cc} \mathbf{A}^s & \mathbf{B}^s \\ \mathbf{B}^s & \mathbf{D}^s \end{array} \right] \tag{13}$$

and $\mathbf{A}, \mathbf{B}, \mathbf{D}, \mathbf{E}, \mathbf{F}, \mathbf{H}, \mathbf{A}^s, \mathbf{B}^s, \mathbf{D}^s$ are the stiffnesses given by:

$$(\mathbf{A}, \mathbf{B}, \mathbf{D}, \mathbf{E}, \mathbf{F}, \mathbf{H}) = \int_{-h/2}^{h/2} (1, z, z^2, z^3, z^4, z^6) \mathbf{C}(z) \mathrm{d}z \tag{14a}$$

$$(\mathbf{A}^s, \mathbf{B}^s, \mathbf{D}^s) = \int_{-h/2}^{h/2} (1, z^2, z^4) \mathbf{C}^s(z) \mathrm{d}z \tag{14b}$$

The work done by transverse load is given by:

$$\mathcal{V} = -\int_A qw \mathrm{d}A \tag{15}$$

The kinetic energy is expressed by:

$$\mathcal{K} = \frac{1}{2}\int_A \dot{\mathbf{u}}^T \mathbf{m}\dot{\mathbf{u}}\,\mathrm{d}A \tag{16}$$

where $\mathbf{u}^T = [u \quad v \quad w \quad \theta_x \quad \theta_y \quad \phi_x \quad \phi_y]$, and the dot-superscript convention indicates the differentiation with respect to the time t, and $\mathbf{m}$ is mass matrix which is given by:

$$\mathbf{m} = \begin{bmatrix} m_{11} & 0 & 0 & m_{14} & 0 & m_{16} & 0 \\ 0 & m_{22} & 0 & 0 & m_{25} & 0 & m_{27} \\ 0 & 0 & m_{33} & 0 & 0 & 0 & 0 \\ m_{14} & 0 & 0 & m_{44} & 0 & m_{46} & 0 \\ 0 & m_{25} & 0 & 0 & m_{55} & 0 & m_{57} \\ m_{16} & 0 & 0 & m_{46} & 0 & m_{66} & 0 \\ 0 & m_{27} & 0 & 0 & m_{57} & 0 & m_{77} \end{bmatrix} \tag{17}$$

where

$$m_{11} = m_{22} = m_{33} = I_0, m_{14} = I_0 + cI_3, m_{16} = cI_3 \tag{18a}$$

$$m_{25} = m_{14}, m_{27} = m_{16}, m_{44} = I_2 + 2cI_4 + c^2 I_6, m_{46} = cI_4 + c^2 I_6 \tag{18b}$$

$$m_{55} = m_{44}, m_{57} = m_{46}, m_{66} = c^2 I_6, m_{77} = m_{66} \tag{18c}$$

with

$$(I_0, I_1, I_2, I_3, I_4, I_6) = \int_{-h/2}^{h/2} \rho(z)(1, z, z^2, z^3, z^4, z^6)\,\mathrm{d}z \tag{19}$$

The Lagrangian functional is finally obtained as:

$$\Pi = \frac{1}{2}\int_A \left(\boldsymbol{\epsilon}_p^T \mathbf{D}^* \boldsymbol{\epsilon}_p + \boldsymbol{\epsilon}_s^T \mathbf{D}_s^* \boldsymbol{\epsilon}_s\right) dA - \int_A qw\mathrm{d}A - \frac{1}{2}\int_A \dot{\mathbf{u}}^T \mathbf{m}\dot{\mathbf{u}}\,\mathrm{d}A \tag{20}$$

2.4. Formulation of finite element method for FG plates

Discretize the bounded domain Ω of plates into N_e finite elements such that $\Omega = \cup_{e=1}^{N_e}\Omega_e$ and $\Omega_i \cap \Omega_j = \emptyset$ with $i \neq j$. The finite element displacements are approximated according to the associated

node displacements as:

$$\mathbf{u} = \sum_{i=1}^{N_n} \begin{bmatrix} N_i(x) & 0 & 0 & 0 & 0 & 0 \\ 0 & N_i(x) & 0 & 0 & 0 & 0 \\ 0 & 0 & N_i(x) & 0 & 0 & 0 \\ 0 & 0 & 0 & N_i(x) & 0 & 0 \\ 0 & 0 & 0 & 0 & N_i(x) & 0 \\ 0 & 0 & 0 & 0 & 0 & N_i(x) \end{bmatrix} \mathbf{d}_i = \mathbf{N}\mathbf{d} \tag{21}$$

where N_n is the total number of nodes of problem domain discretized; N_i(x) is shape function at the ith node; $\mathbf{d}_i^T = [u_i \quad v_i \quad w_i \quad \theta_{xi} \quad \theta_{yi} \quad \phi_{xi} \quad \phi_{yi}]$ is the displacement vector of the nodal degrees of freedom of $\mathbf{u}$ associated to the ith node, respectively. The membrane, bending and shear strains can be then expressed in the matrix forms as:

$$\boldsymbol{\epsilon}^{(0)} = \sum_i \mathbf{B}_i^m \mathbf{d}_i, \boldsymbol{\epsilon}^{(1)} = \sum_i \mathbf{B}_{1i}^b \mathbf{d}_i, \boldsymbol{\epsilon}^{(2)} = \sum_i \mathbf{B}_{2i}^b \mathbf{d}_i \tag{22a}$$

$$\boldsymbol{\gamma}^{(0)} = \sum_i \mathbf{B}_{0i}^s \mathbf{d}_i, \boldsymbol{\gamma}^{(1)} = \sum_i \mathbf{B}_{1i}^s \mathbf{d}_i \tag{22b}$$

where

$$\mathbf{B}_i^m = \begin{bmatrix} N_{i,x} & 0 & 0 & 0 & 0 & 0 & 0 \\ 0 & N_{i,y} & 0 & 0 & 0 & 0 & 0 \\ N_{i,y} & 0 & N_{i,x} & 0 & 0 & 0 & 0 \end{bmatrix} \tag{23a}$$

$$\mathbf{B}_{1i}^b = \begin{bmatrix} 0 & 0 & 0 & N_{i,x} & 0 & 0 & 0 \\ 0 & 0 & 0 & 0 & N_{i,y} & 0 & 0 \\ 0 & 0 & 0 & N_{i,y} & N_{i,x} & 0 & 0 \end{bmatrix} \tag{23b}$$

$$\mathbf{B}_{2i}^b = c \begin{bmatrix} 0 & 0 & 0 & N_{i,x} & 0 & N_{i,x} & 0 \\ 0 & 0 & 0 & 0 & N_{i,y} & 0 & N_{i,y} \\ 0 & 0 & 0 & N_{i,y} & N_{i,x} & N_{i,y} & N_{i,x} \end{bmatrix} \tag{23c}$$

$$\mathbf{B}_{0i}^s = \begin{bmatrix} 0 & 0 & N_{i,x} & N_i & 0 & 0 & 0 \\ 0 & 0 & N_{i,y} & 0 & N_i & 0 & 0 \end{bmatrix} \tag{23d}$$

$$\mathbf{B}_{1i}^s = \begin{bmatrix} 0 & 0 & 0 & N_i & 0 & N_i & 0 \\ 0 & 0 & 0 & 0 & N_i & 0 & N_i \end{bmatrix} \tag{23e}$$

Substituting Eqs. (22) and (21) into Eq. (20) yields:

$$\Pi = \frac{1}{2}\mathbf{d}^T \left[\int_A \left(\mathbf{B}^T \mathbf{D}^* \mathbf{B} + \mathbf{S}^T \mathbf{D}_s^* \mathbf{S} \right) dA \right] \mathbf{d} - \left(\int_A q \mathbf{N} \mathrm{d}A \right) \mathbf{d} - \frac{1}{2}\dot{\mathbf{d}}^T \left(\int_A \mathbf{N}^T \mathbf{m} \mathbf{N} \, dA \right) \dot{\mathbf{d}} \tag{24}$$

where

$$\mathbf{B}^T = \begin{bmatrix} \mathbf{B}^m & \mathbf{B}_1^b & \mathbf{B}_2^b \end{bmatrix}, \mathbf{S}^T = [\mathbf{B}_0^s \quad \mathbf{B}_1^s] \tag{25}$$

The equations of motion for static and vibration can be derived by Lagrange's equations:

$$\frac{\partial \Pi}{\partial q_i} - \frac{d}{dt}\frac{\partial \Pi}{\partial \dot{q}_i} = 0 \tag{26}$$

where q_i represents the global displacements and $\dot{q}_i$ is its velocity. Substituting Eq. (24) into Eq. (26) leads:

$$\mathbf{K}\mathbf{d} + \mathbf{M}\ddot{\mathbf{d}} = \mathbf{P} \tag{27}$$

where

$$\mathbf{K} = \int_A \left(\mathbf{B}^T \mathbf{D}^* \mathbf{B} + \mathbf{S}^T \mathbf{D}_s^* \mathbf{S}\right) \mathrm{d}A \tag{28a}$$

$$\mathbf{P} = \int_A q\mathbf{N} dA \tag{28b}$$

$$\mathbf{M} = \int_A \mathbf{N}^T \mathbf{m} \mathbf{N} \, \mathrm{d}A \tag{28c}$$

Moreover, the displacements are assumed to vary harmonically with respect to time t and a natural frequency ω, thus $\mathbf{d} = \mathbf{q}e^{i\omega t}$ with $i^2 = -1$, Eq. (27) becomes:

$$(\mathbf{K} - \omega^2 \mathbf{M})\mathbf{q} = \mathbf{P} \tag{29}$$

Eq. (29) is the equations of motion for the static and free vibration problem of FG plates and a computer program can be developed to solve this equation to obtain the deflection, stresses and natural frequencies. However, since the shear locking phenomenon can appear as the plate thickness decreases, many approaches have been proposed. Among those, the mixed interpolation of tensorial components (MITC) approach has been applied successfully as a locking removal technique for plate and shell finite elements ([53–57]. In this paper, the MITC3-triangular finite element [53, 58] and edge-based-strain technique is used.

2.5. Formulation of ES-MITC3 finite element method for FG plates

2.5.1. Formulation of MITC3 based on the C^0-HSDT

The original MICT3 element [53] is applied to FSDT plates in which the problem domain is discretized into N_e three-node triangular elements with 5 degrees of freedom (DOFs) per node $\mathbf{d}_i^T = [u_i \quad v_i \quad w_i \quad \theta_{xi} \quad \theta_{yi}]$. Here, the MICT3 element is extended to the C^0-HSDT plates with 7 DOFs per node $\mathbf{d}_i^T = [u_i \quad v_i \quad w_i \quad \theta_{xi} \quad \theta_{yi} \quad \phi_{xi} \quad \phi_{yi}]$. The displacements and rotations of the plate are

assumed to be linear through ones at three element nodes. Moreover, to circumvent the shear locking phenomenon as the plate thickness decreases, the covariant transverse shear strains in the MITC3 element are separately interpolated from values of the covariant transverse shear strains evaluated at tying points which are the center of the isotropic element edges (Fig. 3). To satisfy the isotropic property of the transverse shear strain fields, their interpolations in the natural coordinates (η,ξ) are followed ([53]):

$$\hat{\epsilon}_{\xi\zeta} = \epsilon^{(1)}_{\xi\zeta} + c_1\eta \tag{30a}$$

$$\hat{\epsilon}_{\eta\zeta} = \epsilon^{(2)}_{\eta\zeta} - c_1\xi \tag{30b}$$

with $c_1 = \epsilon^{(2)}_{\eta\zeta} - \epsilon^{(1)}_{\xi\zeta} - \epsilon^{(3)}_{\eta\zeta} + \epsilon^{(3)}_{\xi\zeta}$. The element strain field associated to typing points is given by:

$$\hat{\boldsymbol{\gamma}}^{(0)} = \hat{\mathbf{B}}^s_{0i-MITC3}\mathbf{d} \tag{31}$$

Finally, the shear matrix $\mathbf{S}$ in Eq. (24) is followed:

$$\hat{\mathbf{S}}^T = \begin{bmatrix} \hat{\mathbf{B}}^s_{0-MITC3} & \mathbf{B}^s_1 \end{bmatrix} \tag{32}$$

2.5.2. Formulation of ES-MITC3 based on the C^0-HSDT

The domain discretization for ES-MITC3 is the same one as that of MITC3 using N_n nodes and N_e triangular elements, the displacements and its associated shape functions used in both elements are hence ensured to be continuous on the whole problem domain. In practice, it is known that the MITC3 enables to calculate the stiffness matrix $\mathbf{K}$ based on the elements while the ES-MITC3 uses the edge-based-strain smoothing technique [68] to compute these matrices. The stiffness matrix $\mathbf{K}$ in the ES-MITC3 are therefore called the smoothed stiffness matrix $\tilde{\mathbf{K}}$. In this process, the finite element mesh is further divided into the smoothing domains Ω_k based on edges of elements such that $\Omega = \cup_{k=1}^{N_{ed}}\Omega_k$ and $\Omega_i \cap \Omega_j = \emptyset$ for $i \neq j$, in which N_{ed} is the total number of edges of all elements in the entire problem domain. For triangular elements, the smoothing domain Ω_k associated with the edge k is created by connecting two endpoints of the edge to centroids of adjacent elements as shown in Fig. 4. The strain smoothing formulation is defined by:

$$\tilde{\boldsymbol{\epsilon}}^h = \int_{\Omega_k} \boldsymbol{\epsilon}^h(\mathbf{x})\phi_k(\mathbf{x})\,\mathrm{d}\Omega \tag{33}$$

where $\phi_k(\mathbf{x})$ is a smoothing function that is positive and normalized to unity $\int_{\Omega_k}\phi_k(\mathbf{x})\,d\Omega = 1$. For simplicity, the smoothing function ϕ_k is chosen to be a step function:

$$\phi_k(\mathbf{x}) = \begin{cases} \frac{1}{A_k} & \mathbf{x} \in \Omega_k \\ 0 & \mathbf{x} \ni \Omega_k \end{cases} \tag{34a}$$

where A_k is the area of the smoothing domain Ω_k. The smoothed in-plane and shear strains over the smoothing domain Ω_k are defined by:

$$\tilde{\boldsymbol{\epsilon}}^{(0)} = \frac{1}{A_k}\int_{\Omega_k}\boldsymbol{\epsilon}^{(0)}\,d\Omega, \tilde{\boldsymbol{\epsilon}}^{(1)} = \frac{1}{A_k}\int_{\Omega_k}\boldsymbol{\epsilon}^{(1)}\,d\Omega, \tilde{\boldsymbol{\epsilon}}^{(2)} = \frac{1}{A_k}\int_{\Omega_k}\boldsymbol{\epsilon}^{(2)}\,\mathrm{d}\Omega \tag{35a}$$

$$\tilde{\boldsymbol{\gamma}}^{(0)} = \frac{1}{A_k}\int_{\Omega_k}\hat{\boldsymbol{\gamma}}^{(0)}\,d\Omega, \tilde{\boldsymbol{\gamma}}^{(1)} = \frac{1}{A_k}\int_{\Omega_k}\boldsymbol{\gamma}^{(1)}\,\mathrm{d}\Omega \tag{35b}$$

Substituting Eq. (22) into Eq. (35), the average strains at edge k can be obtained by the following form:

$$\tilde{\boldsymbol{\epsilon}}^{(0)} = \sum_{j=1}^{N_n^k}\tilde{\mathbf{B}}_j^m\mathbf{d}_j, \tilde{\boldsymbol{\epsilon}}^{(1)} = \sum_{j=1}^{N_n^k}\tilde{\mathbf{B}}_{1j}^b\mathbf{d}_j, \tilde{\boldsymbol{\epsilon}}^{(2)} = \sum_{j=1}^{N_n^k}\tilde{\mathbf{B}}_{2j}^b\mathbf{d}_j \tag{36a}$$

$$\tilde{\boldsymbol{\gamma}}^{(0)} = \sum_{j=1}^{N_n^k}\tilde{\mathbf{B}}_{0j}^s\mathbf{d}_j, \tilde{\boldsymbol{\gamma}}^{(1)} = \sum_{j=1}^{N_n^k}\tilde{\mathbf{B}}_{1j}^s\mathbf{d}_j \tag{36b}$$

where N_n^k is the number of nodes belonging to elements directly connected to edge k (N_n^k=3 for boundary edges and N_n^k=4 for inner edges),

$$\tilde{\mathbf{B}}_j^m = \frac{1}{A_k}\sum_{i=1}^{N_e^k}\frac{1}{3}A_i\mathbf{B}_i^m, \tag{37a}$$

$$\tilde{\mathbf{B}}_{1j}^b = \frac{1}{A_k}\sum_{i=1}^{N_e^k}\frac{1}{3}A_i\mathbf{B}_{1i}^b, \tag{37b}$$

$$\tilde{\mathbf{B}}_{2j}^b = \frac{1}{A_k}\sum_{i=1}^{N_e^k}\frac{1}{3}A_i\mathbf{B}_{2i}^b, \tag{37c}$$

$$\tilde{\mathbf{B}}_{0j}^s = \frac{1}{A_k}\sum_{i=1}^{N_e^k}\frac{1}{3}A_i\hat{\mathbf{B}}_{0i-MITC3}^s \tag{37d}$$

$$\tilde{\mathbf{B}}_{1j}^s = \frac{1}{A_k}\sum_{i=1}^{N_e^k}\frac{1}{3}A_i\mathbf{B}_{1i}^s \tag{37e}$$

with N_e^k is the number of elements attached to the edge k (N_e^k=1 for the boundary edges and N_e^k=2 for inner edges). The global matrix of ES-MITC3 element $\tilde{\mathbf{K}}$ is obtained as follows:

$$\tilde{\mathbf{K}} = \int_A\left(\tilde{\mathbf{B}}^T\mathbf{D}^*\tilde{\mathbf{B}} + \tilde{\mathbf{S}}^T\mathbf{D}_s^*\tilde{\mathbf{S}}\right)\mathrm{d}A \tag{38}$$

where $\tilde{\mathbf{B}}^T = [\tilde{\mathbf{B}}^m \quad \tilde{\mathbf{B}}_1^b \quad \tilde{\mathbf{B}}_2^b]$ and $\tilde{\mathbf{S}}^T = [\tilde{\mathbf{B}}_0^s \quad \tilde{\mathbf{B}}_1^s]$. Solving Eq. (29) in taking into account the stiffness matrix $\tilde{\mathbf{K}}$ in Eq. (38) enables to determine static and free vibration responses of the FG plates.

3. Numerical results and discussion

In this section, a number of numerical examples are conducted to show the validity and accuracy of the proposed approaches. Two types of boundary conditions in four sides of plates are considered: simply supported (SSSS) and clamped (CCCC). The FG plates are made of Al/ZrO_2 and Al/Al_2O_3, whose material properties are given in Table 1. For convenience, the following non-dimensional parameters are used:

$$\begin{aligned}
\bar{u}(z) &= \frac{100h^3E_c}{a^4q_0}u\left(0,\frac{b}{2},z\right), \bar{w} = \frac{10h^3E_c}{a^4q_0}w\left(\frac{a}{2},\frac{b}{2}\right), \hat{w} = \frac{10hE_0}{a^2q_0}w\left(\frac{a}{2},\frac{b}{2}\right), \quad E_0 = 1\,\mathrm{GPa} \\
\bar{\sigma}_{xx}(z) &= \frac{h}{aq_0}\sigma_{xx}\left(\frac{a}{2},\frac{b}{2},z\right), \hat{\sigma}_{xx}(z) = \frac{10h^2}{a^2q_0}\sigma_{xx}\left(\frac{a}{2},\frac{b}{2},z\right) \\
\bar{\sigma}_{xy}(z) &= \frac{h}{aq_0}\sigma_{xx}\left(0,0,z\right), \bar{\sigma}_{xz}(z) = \frac{h}{aq_0}\sigma_{xz}\left(0,\frac{b}{2},z\right) \\
\bar{\omega} &= \frac{\omega ab}{\pi^2 h}\sqrt{\frac{12(1-\nu_c^2)\rho_c}{E_c}}, \hat{\omega} = \frac{\omega a^2}{h}\sqrt{\frac{\rho_0}{E_0}}, \quad \rho_o = 1\,\mathrm{kg/m^3}
\end{aligned} \tag{39}$$

For convergence check, Table 2 presents the deflection, stress and fundamental frequency of SSSS isotropic FG plates with p=1 and side-to-thickness ratio a/h=10. It is observed that an accurate solution can be obtained with the meshing 28× 28, thus, this mesh size is used in the following examples. **Moreover, in order to verify the efficiency of present theory in preventing locking phenomena, Table 3 presents the normalized center deflections of isotropic square plates under uniform loading. They are calculated with various side-to-thickness ratios up to a/h=10000, and compared to earlier studies. It can be seen that the proposed ES-MITC3 finite element prevents shear looking, and that they are in excellent agreement with those obtained from [69] and [70]. In addition, the normalized center deflections of $(0^o/90^o/0^o)$ laminated composite square plates subjected to a sinusoidal load are reported in Table 4. They are compared to solutions derived from Carrera et al. [71] for different ratios of a/h. Good agreements between the present solutions and those derived from [71] are observed.**

3.1. Bending analysis

For verification purpose, the displacements and stresses of Al/Al_2O_3 SSSS square plates of Type A and Type B under sinusoidal loads are given in Tables 5, 6 and 7 along with those from sinusoidal shear deformation theory (SSDT) [16], HSDT [21], quasi-3D theories ([25], [26], [28], [37], [39]). It can be seen that the present results are better predictions with those from quasi-3D theories ([25],

[26], [28], [37], [39]) than SSDT [16] and HSDT [21] in many cases. **Table 6 also shows that there are deviations between the normalized membrane stresses of present theory and those from SSDT [16], HSDT [21] with those derived from CUF [65]. These differences are significantly large for thick plates and CUF with** $\epsilon_{zz} = 0$. The variation of axial and transverse shear stresses through the plate thickness for various values of the power-law index and thickness ratio of layers is plotted in Figs. 6a and 6b. Moreover, the deflection and axial stress of Al/ZrO_2 CCCC and SSSS plates of Type C for different thickness ratio of layers are presented in Tables 8 and 9. Again, a good agreement between the present solutions and those from quasi-3D theories ([37], [42]) is found.

3.2. Vibration analysis

The fundamental frequencies of Al^*/ZrO_2 SSSS square plates of Type A and Al/Al_2O_3 SSSS, CCCC plates of Type B are reported in Tables 10 and 11. The results are compared to those obtained from [36] and [44] based a 3D model. Good agreements between the models are again found, even for thick plates. Figure 5 displays first three modes of Al^*/ZrO_2 SSSS square plates with a/h=10, p=1. It can be seen that transverse deflected shapes are appeared in the modes. Furthermore, the fundamental frequencies of Al/Al_2O_3 plates, that is composed of a mixture of metal located at the top surface and ceramic at the bottom one, are additionally considered in Table 12. They are compared to those obtained from HSDTs [48] with 9 and 13 unknowns. The results are calculated for three side-to-thickness ratio a/h=5, 10 and 100 and three thickness ratio of layers (1-1-1,1-2-1 and 2 -2-1). Finally, Tables 13 and 14 contain the fundamental frequencies of Al/Al_2O_3 plates of Type C of present study along with those by SSDT [43], HSDT [45], quasi-3D ([42], [49]) and 3D [44]. Again, an excellent agreement with previous results is found. Figure 7 shows the fundamental frequencies of sandwich plates with respect to the power-law index and side-to-thickness ratio. As p and a/h increase, the results decrease. Their lowest and highest values correspond to the (1-0-1) and (1-2-1) plates, respectively.

4. Conclusions

This paper proposed static and free vibration analysis of isotropic and functionally graded sandwich plates using a higher-order shear deformation theory. Plate mid-plane is divided into three-node triangle element meshing with 7 degree-of-freedoms per nodes that only requires C^0-type continuity. Triangle elements will be divided into three sub-triangles within which a MITC3-element is applied to calculate the strains, and then an edge-based-strain smoothing technique is considered. Numerical results for isotropic and functionally graded sandwich plates with different boundary conditions are

proposed to validate the developed theory and to investigate effects of material distribution, side-to-thickness ratio and thickness ratio of layers on the deflection, stresses and natural frequencies of the plates. The obtained numerical results showed that the present theory is efficient and accurate for static and vibration analysis of isotropic and functionally graded sandwich plates.

Acknowledgements

This research is funded by Vietnam National Foundation for Science and Technology Development (NAFOSTED) under Grant No. 107.02-2015.07.

References

[1] M. Mohammadi, A. Saidi, E. Jomehzadeh, Levy solution for buckling analysis of functionally graded rectangular plates, Applied Composite Materials 17 (2010) 81–93.

[2] G. N. Praveen, J. N. Reddy, Nonlinear transient thermoelastic analysis of functionally graded ceramic-metal plates, International Journal of Solids and Structures 35 (1998) 4457–4476.

[3] L. D. Croce, P. Venini, Finite elements for functionally graded Reissner-Mindlin plates, Computer Methods in Applied Mechanics and Engineering 193 (2004) 705–725.

[4] T.-K. Nguyen, K. Sab, G. Bonnet, Shear correction factors for functionally graded plates, Mechanics of Advanced Materials and Structures 14 (8) (2007) 567–575.

[5] T. K. Nguyen, K. Sab, G. Bonnet, First-order shear deformation plate models for functionally graded materials, Composite Structures 83 (2008) 25–36.

[6] T.-K. Nguyen, T. P. Vo, H.-T. Thai, Vibration and buckling analysis of functionally graded sandwich plates with improved transverse shear stiffness based on the first-order shear deformation theory, Proceedings of the Institution of Mechanical Engineers, Part C: Journal of Mechanical Engineering Science 228 (12) (2014) 2110–2131.

[7] X. Zhao, Y. Y. Lee, K. M. Liew, Mechanical and thermal buckling analysis of functionally graded plates, Composite Structures 90 (2009) 161–171.

[8] X. Zhao, Y. Y. Lee, K. M. Liew, Free vibration analysis of functionally graded plates using the element-free kp-Ritz method, Journal of Sound and Vibration 319 (2009) 918–939.

[9] S. Hosseini-Hashemi, M. Fadaee, S. R. Atashipour, A new exact analytical approach for free vibration of Reissner-Mindlin functionally graded rectangular plates, International Journal of Mechanical Sciences 53 (2011) 11–22.

[10] A. Naderi, A. Saidi, On pre-buckling configuration of functionally graded Mindlin rectangular plates, Mechanics Research Communications 37 (2010) 535–538.

[11] J. N. Reddy, Analysis of functionally graded plates, International Journal for Numerical Methods in Engineering 47 (2000) 663–684.

[12] S. Pradyumna, J. N. Bandyopadhyay, Free vibration analysis of functionally graded curved panels using a higher-order finite element formulation, Journal of Sound and Vibration 318 (2008) 176–192.

[13] D. K. Jha, T. Kant, R. K. Singh, Free vibration response of functionally graded thick plates with shear and normal deformations effects, Composite Structures 96 (2013) 799–823.

[14] J. N. Reddy, A general nonlinear third-order theory of functionally graded plates, International Journal of Aerospace and Lightweight Structures 1 (2011) 1–21.

[15] M. Talha, B. N. Singh, Static response and free vibration analysis of FGM plates using higher order shear deformation theory, Applied Mathematical Modelling 34 (2010) 3991–4011.

[16] A. M. Zenkour, Generalized shear deformation theory for bending analysis of functionally graded materials, Applied Mathematical Modelling 30 (2006) 67–84.

[17] A. M. Zenkour, A simple four-unknown refined theory for bending analysis of functionally graded plates, Applied Mathematical Modelling 37 (20-21) (2013) 9041 – 9051.

[18] H. Matsunaga, Free vibration and stability of functionally graded plates according to a 2-D higher-order deformation theory, Composite Structures 82 (2008) 499–512.

[19] H. T. Thai, S. E. Kim, A simple higher-order shear deformation theory for bending and free vibration analysis of functionally graded plates, Composite Structures 96 (2013) 165–173.

[20] H. T. Thai, D. H. Choi, An efficient and simple refined theory for buckling analysis of functionally graded plates, Applied Mathematical Modelling 36 (2012) 1008–1022.

[21] J. L. Mantari, A. S. Oktem, O. G. Soares, Bending response of functionally graded plates by using a new higher order shear deformation theory, Composite Structures 94 (2012) 714–723.

[22] V.-H. Nguyen, T.-K. Nguyen, H.-T. Thai, T. P. Vo, A new inverse trigonometric shear deformation theory for isotropic and functionally graded sandwich plates, Composites Part B: Engineering 66 (2014) 233 – 246.

[23] T.-K. Nguyen, A higher-order hyperbolic shear deformation plate model for analysis of functionally graded materials, International Journal of Mechanics and Materials in Design 11 (2) (2015) 203–219.

[24] T.-K. Nguyen, H.-T. Thai, T. P. Vo, A refined higher-order shear deformation theory for bending, vibration and buckling analysis of functionally graded sandwich plates, Steel and Composite Structures, An International Journal 18 (1) (2015) 91–120.

[25] E. Carrera, S. Brischetto, A. Robaldo, Variable kinematic model for the analysis of functionally graded material plates, AIAA Journal 46 (1) (2008) 194 – 203.

[26] C.-P. Wu, K.-H. Chiu, Y.-M. Wang, Rmvt-based meshless collocation and element-free galerkin methods for the quasi-3d analysis of multilayered composite and {FGM} plates, Composite Structures 93 (2) (2011) 923 – 943.

[27] A. M. A. Neves, A. J. M. Ferreira, E. Carrera, M. Cinefra, C. M. C. Roque, R. M. N. Jorge, C. M. M. Soares, A quasi-3D hyperbolic shear deformation theory for the static and free vibration analysis of functionally graded plates, Composite Structures 94 (2012) 1814–1825.

[28] A. M. A. Neves, A. J. M. Ferreira, E. Carrera, C. M. C. Roque, M. Cinefra, R. M. N. Jorge, C. M. M. Soares, A quasi-3D sinusoidal shear deformation theory for the static and free vibration analysis of functionally graded plates, Composites Part B: Engineering 43 (2012) 711–725.

[29] J. L. Mantari, C. G. Soares, Generalized hybrid quasi-3D shear deformation theory for the static analysis of advanced composite plates, Composite Structures 94 (8) (2012) 2561 – 2575.

[30] J. L. Mantari, C. G. Soares, A novel higher-order shear deformation theory with stretching effect for functionally graded plates, Composites Part B: Engineering 45 (1) (2013) 268 – 281.

[31] C. Chen, C. Hsu, G. Tzou, Vibration and stability of functionally graded plates based on a higher-order deformation theory, Journal of Reinforced Plastics and Composites 28 (2009) 1215–1234.

[32] D. K. Jha, T. Kant, R. K. Singh, Free vibration response of functionally graded thick plates with shear and normal deformations effects, Composite Structures 96 (2013) 799–823.

[33] H.-T. Thai, S.-E. Kim, A simple quasi-3D sinusoidal shear deformation theory for functionally graded plates, Composite Structures 99 (2013) 172 – 180.

[34] H.-T. Thai, T. P. Vo, T. Q. Bui, T.-K. Nguyen, A quasi-3d hyperbolic shear deformation theory for functionally graded plates, Acta Mechanica 225 (3) (2014) 951–964.

[35] A. Zenkour, Benchmark trigonometric and 3-d elasticity solutions for an exponentially graded thick rectangular plate, Archive of Applied Mechanics 77 (4) (2007) 197–214.

[36] B. Uymaz, M. Aydogdu, Three-dimensional vibration analyses of functionally graded plates under various boundary conditions, Journal of Reinforced Plastics and Composites 26 (18) (2007) 1847–1863.

[37] A. M. A. Neves, A. J. M. Ferreira, E. Carrera, M. Cinefra, C. M. C. Roque, R. M. N. Jorge, C. M. M. Soares, Static, free vibration and buckling analysis of isotropic and sandwich functionally graded plates using a quasi-3D higher-order shear deformation theory and a meshless technique, Composites Part B: Engineering 44 (2013) 657–674.

[38] A. M. Zenkour, A comprehensive analysis of functionally graded sandwich plates: Part 1 Deflection and stresses, International Journal of Solids and Structures 42 (2005) 5224–5242.

[39] E. Carrera, S. Brischetto, M. Cinefra, M. Soave, Effects of thickness stretching in functionally graded plates and shells, Composites Part B: Engineering 42 (2) (2011) 123 – 133.

[40] A. M. Zenkour, Bending analysis of functionally graded sandwich plates using a simple four-unknown shear and normal deformations theory, Journal of Sandwich Structures and Materials 15 (6) (2013) 629–656.

[41] H.-T. Thai, T.-K. Nguyen, T. P. Vo, J. Lee, Analysis of functionally graded sandwich plates using a new first-order shear deformation theory, European Journal of Mechanics - A/Solids 45 (2014) 211 – 225.

[42] A. Bessaim, M. S. Houari, A. Tounsi, S. Mahmoud, E. A. Adda Bedia, A new higher-order shear and normal deformation theory for the static and free vibration analysis of sandwich plates with functionally graded isotropic face sheets, Journal of Sandwich Structures and Materials 15 (6) (2013) 671–703.

[43] A. M. Zenkour, A comprehensive analysis of functionally graded sandwich plates: Part 2 - Buckling and free vibration, International Journal of Solids and Structures 42 (2005) 5243–5258.

[44] Q. Li, V. P. Iu, K. P. Kou, Three-dimensional vibration analysis of functionally graded material sandwich plates, Journal of Sound and Vibration 311 (2008) 498–515.

[45] N. E. Meiche, A. Tounsi, N. Ziane, I. Mechab, E. A. Adda.Bedia, A new hyperbolic shear deformation theory for buckling and vibration of functionally graded sandwich plate, International Journal of Mechanical Sciences 53 (4) (2011) 237 – 247.

[46] M. Sobhy, Buckling and free vibration of exponentially graded sandwich plates resting on elastic foundations under various boundary conditions, Composite Structures 99 (2013) 76 – 87.

[47] S. Xiang, Y. Jin, Z. Bi, S. Jiang, M. S. Yang, A n-order shear deformation theory for free vibration of functionally graded and composite sandwich plates, Composite Structures 93 (2011) 2826–2832.

[48] S. Natarajan, G. Manickam, Bending and vibration of functionally graded material sandwich plates using an accurate theory, Finite Elements in Analysis and Design 57 (2012) 32 – 42.

[49] A. Neves, A. Ferreira, E. Carrera, M. Cinefra, R. Jorge, C. Soares, Buckling analysis of sandwich plates with functionally graded skins using a new quasi-3d hyperbolic sine shear deformation theory and collocation with radial basis functions, Journal of Applied Mathematics and Mechanics 92 (2012) 749766.

[50] C. H. Thai, S. Kulasegaram, L. V. Tran, H. Nguyen-Xuan, Generalized shear deformation theory for functionally graded isotropic and sandwich plates based on isogeometric approach, Computers and Structures 141 (2014) 94–112.

[51] P. Phung-Van, M. Abdel-Wahab, K. Liew, S. Bordas, H. Nguyen-Xuan, Isogeometric analysis of functionally graded carbon nanotube-reinforced composite plates using higher-order shear deformation theory, Composite Structures 123 (2015) 137–149.

[52] C. H. Thai, V. N. Do, H. Nguyen-Xuan, An improved moving kriging-based meshfree method for static, dynamic and buckling analyses of functionally graded isotropic and sandwich plates, Engineering Analysis with Boundary Elements 64 (2016) 122–136.

[53] P.-S. Lee, K.-J. Bathe, Development of MITC isotropic triangular shell finite elements, Computers and Structures 82 (1112) (2004) 945 – 962.

[54] E. N. Dvorkin, K. Bathe, A continuum mechanics based fournode shell element for general nonlinear analysis, Engineering Computations 1 (1) (1984) 77–88.

[55] M. L. Bucalem, K.-J. Bathe, Higher-order mitc general shell elements, International Journal for Numerical Methods in Engineering 36 (21) (1993) 3729–3754.

[56] T. Chau-Dinh, G. Zi, P.-S. Lee, T. Rabczuk, J.-H. Song, Phantom-node method for shell models with arbitrary cracks, Computers and Structures 9293 (2012) 242 – 256.

[57] Y. Lee, K. Yoon, P.-S. Lee, Improving the MITC3 shell finite element by using the hellingerreissner principle, Computers and Structures 110111 (2012) 93 – 106.

[58] P.-S. Lee, H.-C. Noh, K.-J. Bathe, Insight into 3-node triangular shell finite elements: the effects of element isotropy and mesh patterns, Computers & Structures 85 (78) (2007) 404 – 418.

[59] G. Liu, N. Trung, Smoothed Finite Element Methods, Taylor & Francis, 2010.
URL https://books.google.ca/books?id=9TdHtwAACAAJ

[60] G. R. Liu, K. Y. Dai, T. T. Nguyen, A smoothed finite element method for mechanics problems, Computational Mechanics 39 (6) (2007) 859–877.

[61] G. Liu, T. Nguyen-Thoi, H. Nguyen-Xuan, K. Lam, A node-based smoothed finite element method (ns-fem) for upper bound solutions to solid mechanics problems, Computers & Structures 87 (12) (2009) 14 – 26.

[62] G. Liu, T. Nguyen-Thoi, K. Lam, An edge-based smoothed finite element method (es-fem) for static, free and forced vibration analyses of solids, Journal of Sound and Vibration 320 (45) (2009) 1100 – 1130.

[63] T. Nguyen-Thoi, G. R. Liu, K. Y. Lam, G. Y. Zhang, A face-based smoothed finite element method (fs-fem) for 3d linear and geometrically non-linear solid mechanics problems using 4-node tetrahedral elements, International Journal for Numerical Methods in Engineering 78 (3) (2009) 324–353.

[64] W. Koiter, T. H. D. L. voor Toegepaste Mechanica, A Consistent First Approximation in the General Theory of Thin Elastic Shells: Foundations and linear theory, no. phn 1, Laboratorium voor Toegepaste Mechanica der Technische Hogeschool, 1959.
URL https://books.google.com.vn/books?id=h5TZtgAACAAJ

[65] E. Carrera, F. Miglioretti, M. Petrolo, Accuracy of refined finite elements for laminated plate analysis, Composite Structures 93 (5) (2011) 1311 – 1327.

[66] A. J. M. Ferreira, C. M. d. C. Roque, E. Carrera, M. Cinefra, O. Polit, Analysis of sandwich plates by radial basis functions collocation, according to murakami's zig-zag theory, Journal of Sandwich Structures and Materials 14 (5) (2012) 505–524.

[67] C. Shankara, N. Iyengar, A c0 element for the free vibration analysis of laminated composite plates, Journal of Sound and Vibration 191 (5) (1996) 721 – 738.

[68] J.-S. Chen, C.-T. Wu, S. Yoon, Y. You, A stabilized conforming nodal integration for galerkin mesh-free methods, International Journal for Numerical Methods in Engineering 50 (2) (2001) 435–466.

[69] H. Nguyen-Xuan, T. Rabczuk, S. Bordas, J. Debongnie, A smoothed finite element method for plate analysis, Computer Methods in Applied Mechanics and Engineering 197 (1316) (2008) 1184 – 1203.

[70] R. L. Taylor, F. Auricchio, Linked interpolation for reissner-mindlin plate elements: Part iia simple triangle, International Journal for Numerical Methods in Engineering 36 (18) (1993) 3057–3066.

[71] E. Carrera, M. Cinefra, P. Nali, {MITC} technique extended to variable kinematic multilayered plate elements, Composite Structures 92 (8) (2010) 1888 – 1895.

CAPTIONS OF TABLES

Table 1: Material properties of metal and ceramic.

Table 2: Convergence of static and vibration responses of Al/Al_2O_3 simply supported square plates (SSSS, a/h=10, Type A).

Table 3: Nondimensional center deflections $100w\left(\frac{a}{2},\frac{b}{2}\right)D/q_0a^4$, $D=\frac{Eh^3}{12(1-\nu^2)}$ of simply supported isotropic plates under uniform loads.

Table 4: Nondimensional center deflections $100w\left(\frac{a}{2},\frac{b}{2}\right)E_Th^3/q_0a^4$ of $(0^o/90^o/0^o)$ simply supported laminated composite plates under sinusoidal loads.

Table 5: Comparison of the nondimensional stress and displacements of Al/Al_2O_3 simply supported square plates (SSSS, a/h=10, Type A).

Table 6: Nondimensional membrane stress $\bar{\sigma}_{xx}$ and deflection $\bar{w}$ of Al/Al_2O_3 simply supported square FG plates (SSSS, Type A).

Table 7: Comparison of the nondimensional stress and displacements of Al/Al_2O_3 simply supported square plates (SSSS, a/h=10, Type B).

Table 8: Nondimensional center deflections ($\hat{w}$) of Al/ZrO_2 sandwich clamped square plates (CCCC, Type C).

Table 9: Nondimensional axial stress ($\hat{\sigma}_{xx}$) of Al/ZrO_2 sandwich simply supported square plates (SSSS, a/h=10, Type C).

Table 10: Comparison of the nondimensional fundamental frequency ($\bar{\omega}$) of Al^*/ZrO_2 simply supported square plates (SSSS, Type A).

Table 11: Nondimensional fundamental frequency ($\hat{\omega}$) of Al/Al_2O_3 square plates (Type B, 1-8-1).

Table 12: Comparison of the nondimensional fundamental frequency ($\hat{\omega}$) of Al/Al_2O_3 simply supported square plates (SSSS, Type B).

Table 13: Nondimensional fundamental frequency ($\hat{\omega}$) of Al/Al_2O_3 sandwich simply supported square plates (SSSS, a/h=10, Type C).

Table 14: Nondimensional fundamental frequency ($\hat{\omega}$) of Al/Al_2O_3 sandwich clamped square plates (CCCC, Type C).

CAPTIONS OF FIGURES

Figure 1: Geometry of functionally graded plates and its sections.

Figure 2: 1-2-1 sandwich plates for several power-law index (p).

Figure 3: Typing points

Figure 4: Smoothing domain associated with edge k

Figure 5: First three shape modes of Al^*/ZrO_2 simply supported square plates (a/h=10, p=1, Type A).

Figure 6: Nondimensional membrane stress $\bar{\sigma}_{xx}$ and transverse shear stress $\bar{\sigma}_{xz}$ through the thickness direction of Al/Al_2O_3 simply supported square plates subjected to sinusoidal load (a/h=10, Type B).

Figure 7: Effect of the power-law index p and side-to-thickness ratio on the nondimensional fundamental frequency ($\hat{\omega}$) of Al/Al_2O_3 simply supported square plates (Type C).

Table 1: Material properties of metal and ceramic

Material	Young's modulus (GPa)	Mass density (kg/m^3)	Poisson's ratio
Aluminum (Al^*)	70	2702	0.3
Aluminum (Al)	70	2707	0.3
Zirconia (ZrO_2)	151	3000	0.3
Alumina (Al_2O_3)	380	3800	0.3

Table 2: Convergence of static and vibration responses of Al/Al_2O_3 simply supported square plates (SSSS, a/h=10, Type A)

Responses	Meshing					
	4×4	8×8	16×16	24×24	28×28	32×32
$\bar{w}$	0.4967	0.5690	0.5842	0.5868	0.5874	0.5878
$\bar{\sigma}_{xx}(h/3)$	1.1368	1.4015	1.4675	1.4799	1.4825	1.4842
$\hat{\omega}$	0.1307	0.1497	0.1537	0.1544	0.1545	0.1546

Table 3: Nondimensional center deflections $100w\left(\frac{a}{2},\frac{b}{2}\right)D/q_0a^4$, $D=\frac{Eh^3}{12(1-\nu^2)}$ of simply supported isotropic plates under uniform loads.

BC	Theory	a/h			
		10	100	1000	10000
SSSS	Present	0.4272	0.4064	0.4062	0.4062
	Nguyen et al. (MITC4) [69]	0.4273	0.4064	0.4062	0.4062
	Nguyen et al. (MISC1) [69]	0.4273	0.4065	0.4063	0.4063
	Exact [70]	0.4273	0.4064	0.4062	0.4062
CCCC	Present	0.1505	0.1268	0.1265	0.1265
	Nguyen et al. (MITC4) [69]	0.1504	0.1268	0.1265	0.1265
	Nguyen et al. (MISC1) [69]	0.1505	0.1268	0.1265	0.1265
	Exact [70]	0.1499	0.1267	0.1265	0.1265

Table 4: Nondimensional center deflections $100w\left(\frac{a}{2},\frac{b}{2}\right)E_2h^3/q_0a^4$ of $(0^o/90^o/0^o)$ simply supported laminated composite plates under sinusoidal loads.

Theory	a/h				
	10	50	100	500	1000
Present	0.9750	0.7856	0.7740	0.7747	0.7655
Carrera et al. (MITC4)[71]	0.9754	0.7737	0.7672	0.7650	0.7632

Table 5: Comparison of the nondimensional stress and displacements of Al/Al_2O_3 simply supported square plates (SSSS, a/h=10, Type A).

p	Theory	$\bar{u}(-h/4)$	$\bar{w}$	$\bar{\sigma}_{xx}(h/3)$	$\bar{\sigma}_{xy}(-h/3)$	$\bar{\sigma}_{xz}(h/6)$
1	Present	0.6402	0.5874	1.4825	0.6080	0.2597
	Quasi-3D [25]	0.6436	0.5875	1.5062	0.6081	0.2510
	Quasi-3D [26]	0.6436	0.5876	1.5061	0.6112	0.2511
	SSDT [16]	0.6626	0.5889	1.4894	0.6110	0.2622
	HSDT [21]	0.6398	0.5880	1.4888	0.6109	0.2566
2	Present	0.8970	0.7553	1.3890	0.5414	0.2755
	Quasi-3D [25]	0.9012	0.7570	1.4147	0.5421	0.2496
	Quasi-3D [26]	0.9013	0.7571	1.4129	0.5436	0.2495
	SSDT [16]	0.9281	0.7573	1.3954	0.5441	0.2763
	HSDT [21]	0.8957	0.7564	1.3940	0.5438	0.2741
4	Present	1.0488	0.8795	1.1718	0.5639	0.2611
	Quasi-3D [25]	1.0541	0.8823	1.1985	0.5666	0.2362
	Quasi-3D [26]	1.0541	0.8823	1.1941	0.5671	0.2362
	SSDT [16]	1.0941	0.8819	1.1783	0.5667	0.2580
	HSDT [21]	1.0457	0.8814	1.1755	0.5662	0.2623
8	Present	1.0754	0.9723	0.9413	0.5826	0.2041
	Quasi-3D [25]	1.0830	0.9738	0.9687	0.5879	0.2262
	Quasi-3D [26]	1.0830	0.9739	0.9622	0.5883	0.2261
	SSDT [16]	1.1340	0.9750	0.9466	0.5856	0.2121
	HSDT [21]	1.0709	0.9737	0.9431	0.5850	0.2140

Table 6: Nondimensional membrane stress $\bar{\sigma}_{xx}$ and deflection $\bar{w}$ of Al/Al_2O_3 simply supported square FG plates (SSSS, Type A).

p	Theory	$\bar{\sigma}_{xx}(h/3)$			$\bar{w}$		
		a/h=4	10	100	a/h=4	10	100
1	Present	0.5787	1.4825	14.894	0.7271	0.5874	0.5609
	SSDT [16]	-	1.4894	-	-	0.5889	-
	HSDT [21]	-	1.4888	-	-	0.5880	-
	CUF [39] ($\epsilon_{zz} = 0$)	0.7856	2.0068	20.149	0.7289	0.5890	0.5625
	CUF [39] ($\epsilon_{zz} \neq 0$)	0.6221	1.5064	14.969	0.7171	0.5875	0.5625
	Quasi-3D [26]	-	1.5061	-	-	0.5876	-
4	Present	0.4390	1.1719	11.862	1.1593	0.8795	0.8263
	SSDT [16]	-	1.1783	-	-	0.8819	-
	HSDT [21]	-	1.1755	-	-	0.8814	-
	CUF [39] ($\epsilon_{zz} = 0$)	0.5986	1.5874	16.047	1.1673	0.8828	0.8286
	CUF [39] ($\epsilon_{zz} \neq 0$)	0.4877	1.1971	11.923	1.1585	0.8821	0.8286
	Quasi-3D [26]	-	1.1941	-	-	0.8823	-
10	Present	0.3220	0.8730	8.8566	1.3896	1.0061	0.9332
	SSDT [16] ($\epsilon_{zz} = 0$)	-	0.8775	-	-	1.0089	-
	CUF [39] ($\epsilon_{zz} = 0$)	0.4345	1.1807	11.989	1.3925	1.0090	0.9361
	CUF [39] ($\epsilon_{zz} \neq 0$)	0.1478	0.8965	8.9077	1.3745	1.0072	0.9361

Table 7: Comparison of the nondimensional stress and displacements of Al/Al_2O_3 simply supported square plates (SSSS, a/h=10, Type B).

p	Theory	$\bar{u}(-h/4)$	$\bar{w}$	$\bar{\sigma}_{xx}(h/3)$	$\bar{\sigma}_{xy}(-h/3)$	$\bar{\sigma}_{xz}(h/6)$
0	Present	0.3221	0.3726	1.4614	1.0023	0.2202
	Quasi-3D [37]	-	0.3711	-	-	0.2227
0.5	Present	0.5514	0.5216	1.5020	0.8487	0.2451
	Quasi-3D [37]	-	0.5238	-	-	0.2581
1	Present	0.7312	0.6319	1.4493	0.6867	0.2587
	Quasi-3D [39]	-	0.6324	-	-	0.2594
	Quasi-3D [28]	-	0.6305	-	-	0.2788
	Quasi-3D [37]	-	0.6305	-	-	0.2789
4	Present	1.0524	0.8264	0.9522	0.5563	0.2435
	Quasi-3D [39]	-	0.8307	-	-	0.2398
	Quasi-3D [28]	-	0.8202	-	-	0.2778
	Quasi-3D [37]	-	0.8199	-	-	0.2747
10	Present	1.0771	0.8719	0.5582	0.5662	0.1925
	Quasi-3D [39]	-	0.8740	-	-	0.1944
	Quasi-3D [28]	-	0.8650	-	-	0.2059
	Quasi-3D [37]	-	0.8645	-	-	0.2034

Table 8: Nondimensional center deflections ($\hat{w}$) of Al/ZrO_2 sandwich clamped square plates (CCCC, Type C).

h/b	p	Theory	1-0-1	2-1-2	2-1-1	1-1-1	2-2-1	1-2-1
0.01	0	Present	0.0961	0.0961	0.0961	0.0961	0.0961	0.0961
	0.5	Present	0.1356	0.1302	0.1275	0.1259	0.1226	0.1196
	1	Present	0.1601	0.1516	0.1468	0.1445	0.1389	0.1339
	5	Present	0.2025	0.1945	0.1849	0.1844	0.1734	0.1661
	10	Present	0.2061	0.2005	0.1905	0.1915	0.1797	0.1728
0.1	0	Present	0.1156	0.1156	0.1156	0.1156	0.1156	0.1156
		HSDT [24]	0.1128	0.1128	0.1128	0.1128	0.1128	0.1128
	0.5	Present	0.1588	0.1525	0.1497	0.1477	0.1442	0.1410
		HSDT [24]	0.1557	0.1495	0.1467	0.1448	0.1414	0.1381
	1	Present	0.1862	0.1760	0.1709	0.1679	0.1619	0.1563
		HSDT [24]	0.1824	0.1726	0.1675	0.1648	0.1588	0.1535
	5	Present	0.2363	0.2238	0.2136	0.2116	0.1996	0.1909
		HSDT [24]	0.2304	0.2187	0.2091	0.2073	0.1957	0.1878
	10	Present	0.2429	0.2312	0.2204	0.2196	0.2067	0.1983
		HSDT [24]	0.2365	0.2255	0.2156	0.2149	0.2024	0.1949
0.2	0	Present	0.1652	0.1652	0.1652	0.1652	0.1652	0.1652
	0.5	Present	0.2166	0.2080	0.2049	0.2019	0.1981	0.1939
	1	Present	0.2496	0.2351	0.2297	0.2248	0.2182	0.2111
	5	Present	0.3195	0.2935	0.2822	0.2754	0.2619	0.2497
	10	Present	0.3346	0.3046	0.2924	0.2856	0.2709	0.2581

Table 9: Nondimensional axial stress ($\hat{\sigma}_{xx}$) of Al/ZrO_2 sandwich simply supported square plates (SSSS, a/h=10, Type C).

p	Theory	1-0-1	2-1-2	2-1-1	1-1-1	2-2-1	1-2-1
0	Present	1.96556	1.96556	1.96556	1.96556	1.96556	1.96556
	Zenkour [38] (SSDT)	2.05452	2.05452	-	2.05452	2.05452	2.05452
	Zenkour [40] (Quasi-3D)	2.00773	2.00773	-	2.00773	2.00773	2.00773
	Neves et al. [37] (Quasi-3D)	-	2.00660	2.00640	2.00660	2.00650	2.00640
	Bessaim et al. [42] (Quasi-3D)	-	1.99524	1.99524	1.99524	1.99524	1.99524
1.0	Present	1.56840	1.45972	1.34829	1.39036	1.28054	1.28866
	Zenkour [38] (SSDT)	1.58204	1.49859	-	1.42892	1.32342	1.32590
	Zenkour [40] (Quasi-3D)	1.57004	1.48833	-	1.41781	1.30907	1.31204
	Neves et al. [37] (Quasi-3D)	-	1.48130	1.37680	1.41370	1.30920	1.31330
	Bessaim et al. [42] (Quasi-3D)	-	1.46131	1.35053	1.39243	1.28274	1.29030
2.0	Present	1.80135	1.68374	1.51308	1.59049	1.42750	1.44340
	Zenkour [38] (SSDT)	1.82450	1.72412	-	1.63025	1.47387	1.48283
	Zenkour [40] (Quasi-3D)	1.81509	1.72030	-	1.62591	1.46372	1.47421
	Neves et al. [37] (Quasi-3D)	-	1.69940	1.54560	1.60880	1.45430	1.46590
	Bessaim et al. [42] (Quasi-3D)	-	1.68472	1.52101	1.59170	1.42887	1.44497
5.0	Present	1.92800	1.85438	1.65950	1.77191	1.56846	1.59723
	Zenkour [38] (SSDT)	1.99567	1.91547	-	1.81838	1.61477	1.64106
	Zenkour [40] (Quasi-3D)	1.97912	1.91504	-	1.82018	1.60953	1.63906
	Neves et al. [37] (Quasi-3D)	-	1.88380	1.69090	1.79060	1.58930	1.61950
	Bessaim et al. [42] (Quasi-3D)	-	1.87516	1.66856	1.77919	1.56627	1.60203
10.0	Present	1.99493	1.93047	1.71601	1.84567	1.61513	1.66494
	Zenkour [38] (SSDT)	2.03360	1.97313	-	1.88147	1.61979	1.64851
	Zenkour [40] (Quasi-3D)	2.00692	1.97075	-	1.89162	2.18558	1.67350
	Neves et al. [37] (Quasi-3D)	-	1.93970	1.74050	1.85590	1.63950	1.68320
	Bessaim et al. [42] (Quasi-3D)	-	1.93266	1.71835	1.84705	1.61792	1.66754

Table 10: Comparison of the nondimensional fundamental frequency ($\bar{\omega}$) of Al^*/ZrO_2 simply supported square plates (SSSS, Type A).

a/h	Theory	p							
		0	0.1	0.2	0.5	1	2	5	10
2	Present	1.2502	1.2210	1.1960	1.1390	1.0821	1.0268	0.9717	0.9466
	3D [36]	1.2589	1.2296	1.2049	1.1484	1.0913	1.0344	0.9777	0.9507
5	Present	1.7782	1.7270	1.6893	1.6057	1.5293	1.4677	1.4132	1.3764
	3D [36]	1.7748	1.7262	1.6881	1.6031	1.4764	1.4628	1.4106	1.3711
10	Present	1.9426	1.8863	1.8426	1.7488	1.6674	1.6074	1.5578	1.5168
	3D [36]	1.9339	1.8788	1.8357	1.7406	1.6583	1.5968	1.5491	1.5066
20	Present	1.9932	1.9286	1.8822	1.7908	1.7098	1.6507	1.6032	1.5608
	3D [36]	1.9570	1.9261	1.8788	1.7832	1.6999	1.6401	1.5937	1.5491
50	Present	2.0028	1.9274	1.8888	1.8001	1.7188	1.6598	1.6129	1.5700
	3D [36]	1.9974	1.9390	1.8920	1.7944	1.7117	1.6522	1.6062	1.5620
100	Present	2.0050	1.9272	1.8885	1.7999	1.7188	1.6599	1.6132	1.5704
	3D [36]	1.9974	1.9416	1.8920	1.7972	1.7117	1.6552	1.6062	1.5652

Table 11: Nondimensional fundamental frequency ($\hat{\omega}$) of Al/Al_2O_3 square plates (Type B, 1-8-1).

Boundary conditions	h/b	Theory	p				
			0.5	1	2	5	10
SSSS	0.01	Present	1.34091	1.38713	1.44558	1.53261	1.59320
		Li et al. [44] (3D)	1.33931	1.38669	1.44491	1.53143	1.59105
	0.1	Present	1.30037	1.35075	1.41078	1.49640	1.55372
		Li et al. [44] (3D)	1.29751	1.34847	1.40828	1.49309	1.54980
	0.2	Present	1.19521	1.25212	1.31480	1.39697	1.44837
		Li et al. [44] (3D)	1.19580	1.25338	1.31569	1.39567	1.44540
CCCC	0.01	Present	2.45628	2.54032	2.64720	2.80567	2.91465
		Li et al. [44] (3D)	2.45438	2.54149	2.64835	2.80692	2.91611
	0.1	Present	2.24211	2.34552	2.45892	2.60848	2.70317
		Li et al. [44] (3D)	2.24154	2.34606	2.45973	2.60760	2.70070
	0.2	Present	1.85910	1.97572	2.09056	2.22000	2.29087
		Li et al. [44] (3D)	1.86081	1.97993	2.09554	2.22142	2.28896

Table 12: Comparison of the nondimensional fundamental frequency ($\hat{\omega}$) of Al/Al_2O_3 simply supported square plates (SSSS, Type B).

a/h	Theory	1-1-1				1-2-1			2-2-1		
		0	0.5	1	5	0.5	1	5	0.5	1	5
5	Present	1.1072	1.1485	1.1765	1.2125	1.1622	1.1902	1.2686	1.1984	1.2392	1.3283
	HSDT9 [48]	1.1021	1.1449	1.1639	1.2113	1.1597	1.1884	1.2644	1.1965	1.2350	1.3249
	HSDT13 [48]	1.0893	1.1511	1.1701	1.2162	1.1663	1.1952	1.2712	1.2031	1.2421	1.3312
10	Present	1.2040	1.2412	1.2573	1.2951	1.2614	1.2851	1.3523	1.2878	1.3246	1.4196
	HSDT9 [48]	1.2138	1.2373	1.2506	1.2921	1.2578	1.2785	1.3492	1.2846	1.3216	1.4161
	HSDT13 [48]	1.2087	1.2392	1.2524	1.2935	1.2598	1.2806	1.3513	1.2865	1.3238	1.4180
100	Present	1.2652	1.2785	1.2890	1.3276	1.3014	1.3185	1.3864	1.3214	1.3597	1.4559
	HSDT9 [48]	1.2617	1.2751	1.2854	1.3239	1.2981	1.3148	1.3825	1.3198	1.3559	1.4519
	HSDT13 [48]	1.2616	1.2751	1.2854	1.3239	1.2981	1.3148	1.3825	1.3198	1.3559	1.4519

Table 13: Nondimensional fundamental frequency ($\hat{\omega}$) of Al/Al_2O_3 sandwich simply supported square plates (SSSS, a/h=10, Type C).

p	Theory	1-0-1	2-1-2	2-1-1	1-1-1	2-2-1	1-2-1
0	Present	1.82996	1.82996	1.82996	1.82996	1.82996	1.82996
	Zenkour [43] (SSDT)	1.82452	1.82452	1.82452	1.82452	1.82452	1.82452
	Meiche et al. [45] (HSDT)	1.82449	1.82449	1.82449	1.82449	1.82449	1.82449
	Bessaim et al. [42] (Quasi-3D)	1.82682	1.82682	-	1.82682	1.82682	1.82682
	Li et al. [44] (3D)	1.82682	1.82682	-	1.82682	1.82682	1.82682
0.5	Present	1.44753	1.48775	1.51016	1.52316	1.55114	1.57879
	Zenkour [43] (SSDT)	1.44436	1.48418	1.51258	1.51927	1.55202	1.57450
	Meiche et al. [45] (HSDT)	1.44419	1.48405	1.50636	1.51922	1.54714	1.57458
	Bessaim et al. [42] (Quasi-3D)	1.44621	1.48611	-	1.52130	1.55016	1.57670
	Li et al. [44] (3D)	1.44614	1.48608	-	1.52131	1.54926	1.57668
1.0	Present	1.24683	1.30397	1.33732	1.35740	1.39980	1.44368
	Zenkour [43] (SSDT)	1.24335	1.30023	1.34894	1.35339	1.40792	1.43931
	Meiche et al. [45] (HSDT)	1.24310	1.30004	1.33328	1.35331	1.39559	1.43940
	Bessaim et al. [42] (Quasi-3D)	1.24495	1.30195	-	1.35527	1.39987	1.44143
	Li et al . [44] (3D)	1.24470	1.30181	-	1.35523	1.39763	1.44137
5.0	Present	0.94802	0.98388	1.03320	1.04729	1.11199	1.17748
	Zenkour [43] (SSDT)	0.94630	0.98207	1.07445	1.04481	1.14741	1.17399
	Meiche et al. [45] (HSDT)	0.94574	0.98166	1.03033	1.04455	1.10875	1.17397
	Bessaim et al. [42] (Quasi-3D)	0.94716	0.98311	-	1.04613	1.11723	1.17579
	Li et al. [44] (3D)	0.94476	0.98103	-	1.04532	1.10983	1.17567
10.0	Present	0.93054	0.94458	0.99449	0.99769	1.06381	1.12641
	Zenkour [43] (SSDT)	0.92875	0.94332	1.04558	0.99519	1.04154	1.13460
	Meiche et al. [45] (HSDT)	0.92811	0.94275	0.99184	0.99536	1.06081	1.12311
	Bessaim et al. [42] (Quasi-3D)	0.92952	0.94410	-	0.99684	1.07015	1.12486
	Li et al. [44] (3D)	0.92727	0.94078	-	0.99523	1.06104	1.12466

Table 14: Nondimensional fundamental frequency ($\hat{\omega}$) of Al/Al_2O_3 sandwich clamped square plates (CCCC, Type C).

h/b	p	Theory	1-0-1	2-1-2	2-1-1	1-1-1	2-2-1	1-2-1
0.01	0	Present	3.45280	3.45280	3.45280	3.45280	3.45280	3.45280
		Li et al. [44] (3D)	3.45447	3.45447	3.45447	3.45447	3.45447	3.45447
	0.5	Present	2.70385	2.78089	2.84948	2.90462	2.95806	3.22393
		Li et al. [44] (3D)	2.71263	2.78786	2.85535	2.90993	2.96675	3.23192
	1	Present	2.32617	2.43257	2.53379	2.61568	2.69909	3.10729
		Li et al. [44] (3D)	2.32703	2.43347	2.53476	2.61669	2.71273	3.11384
	5	Present	1.76665	1.82803	1.94525	2.06793	2.25305	2.87134
		Li et al. [44] (3D)	1.76711	1.82843	1.94575	2.06851	2.25938	2.87731
	10	Present	1.73862	1.75541	1.85247	1.97736	2.09335	2.81977
		Li et al. [44] (3D)	1.73916	1.75573	1.85287	1.97781	2.09743	2.82561
0.1	0	Present	3.13561	3.13561	3.13561	3.13561	3.13561	3.13561
		Li et al. [44] (3D)	3.13799	3.13799	3.13799	3.13799	3.13799	3.13799
	0.5	Present	2.52313	2.59231	2.65098	2.69559	2.74092	2.95395
		Li et al. [44] (3D)	2.52593	2.59490	2.65356	2.69828	2.74989	2.95839
	1	Present	2.18997	2.29045	2.38082	2.44990	2.52297	2.85877
		Li et al. [44] (3D)	2.19019	2.29107	2.38186	2.45108	2.53978	2.86255
	5	Present	1.67051	1.74592	1.85938	1.96982	2.08304	2.66415
		Li et al. [44] (3D)	1.66187	1.73925	1.85790	1.96719	2.15715	2.66739
	10	Present	1.62965	1.67549	1.77308	1.88712	1.99676	2.62127
		Li et al. [44] (3D)	1.62117	1.66326	1.76860	1.88080	1.99860	2.62431
0.2	0	Present	2.57142	2.57142	2.57142	2.57142	2.57142	2.57142
		Li et al. [44] (3D)	2.57552	2.57552	2.57552	2.57552	2.57552	2.57552
	0.5	Present	2.15479	2.21224	2.25626	2.28573	2.32903	2.45801
		Li et al. [44] (3D)	2.15683	2.21438	2.25866	2.28822	2.33060	2.46042
	1	Present	1.90597	1.99495	2.06602	2.11415	2.18758	2.39488
		Li et al. [44] (3D)	1.90590	1.99492	2.06686	2.11525	2.19019	2.39709
	5	Present	1.44371	1.54845	1.66152	1.74282	1.93751	2.26000
		Li et al. [44] (3D)	1.44469	1.54542	1.66225	1.74700	1.93215	2.26481
	10	Present	1.38793	1.46787	1.58394	1.67647	1.78228	2.23314
		Li et al. [44] (3D)	1.38683	1.46709	1.58209	1.67158	1.78269	2.23526

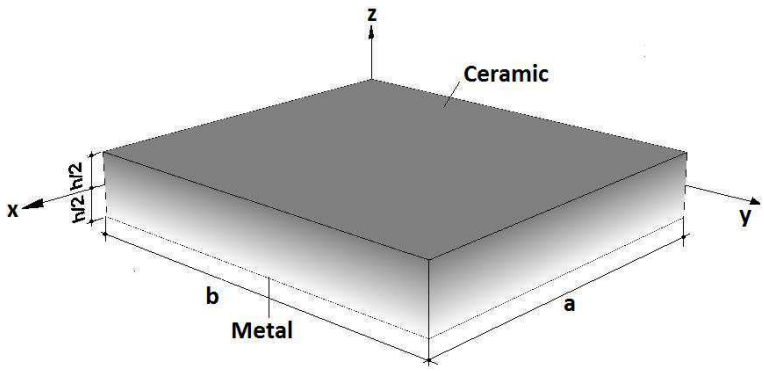

(a) Geometry of a functionally graded plate

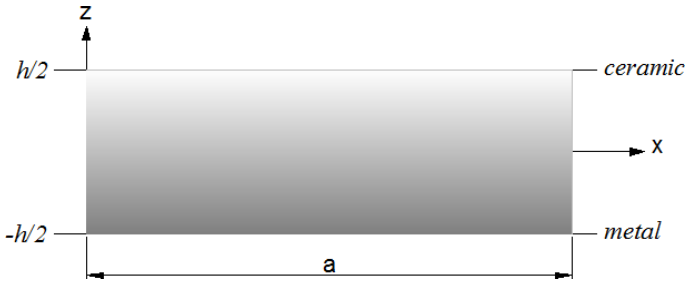

(b) Type A

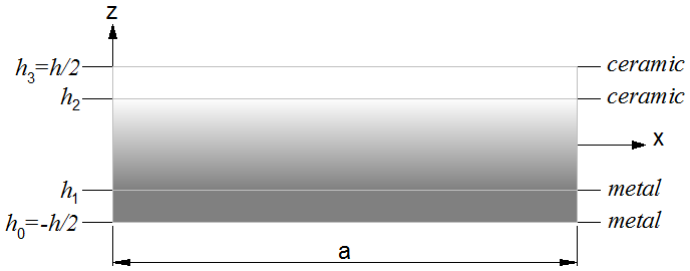

(c) Type B

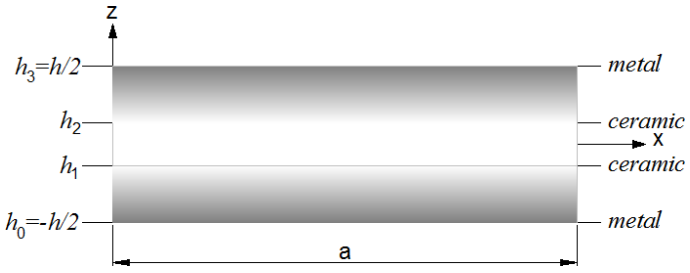

(d) Type C

Figure 1: Geometry of functionally graded plates and its sections.

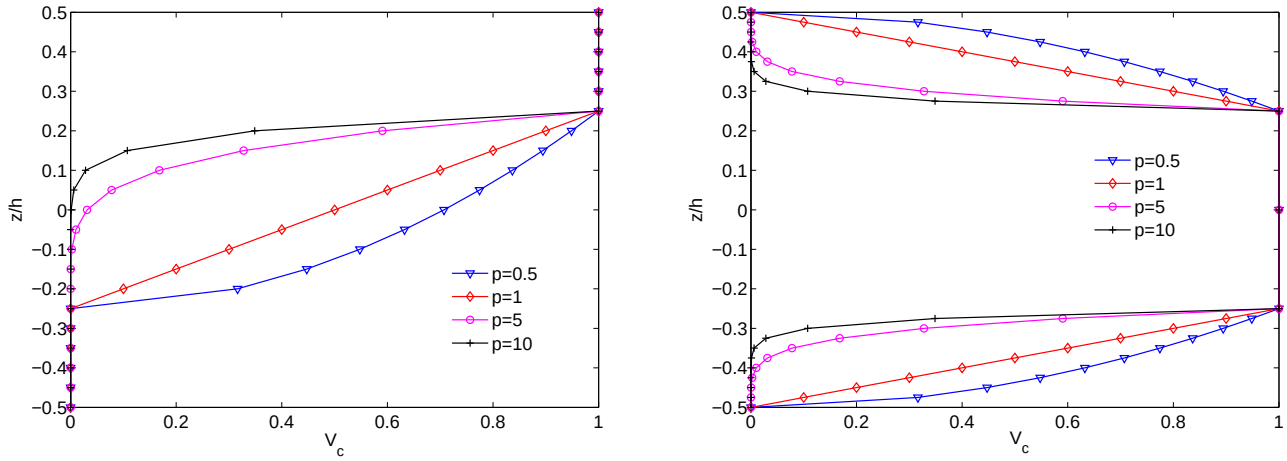

(a) Type B

(b) Type C

Figure 2: 1-2-1 sandwich plates for several power-law index (p).

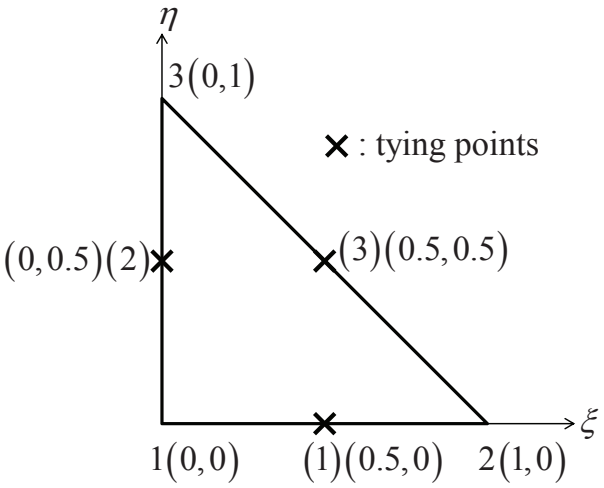

Figure 3: Typing points

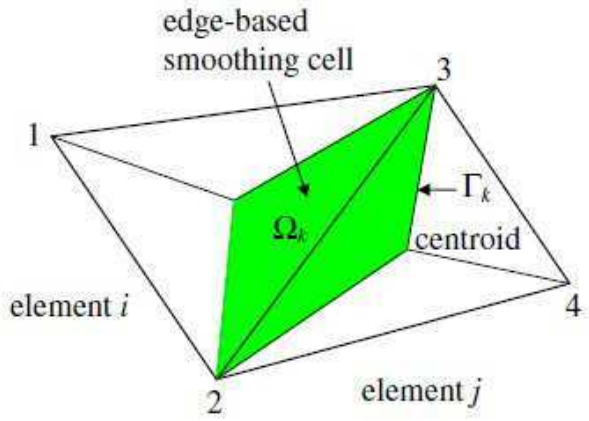

Figure 4: Smoothing domain associated with edge k

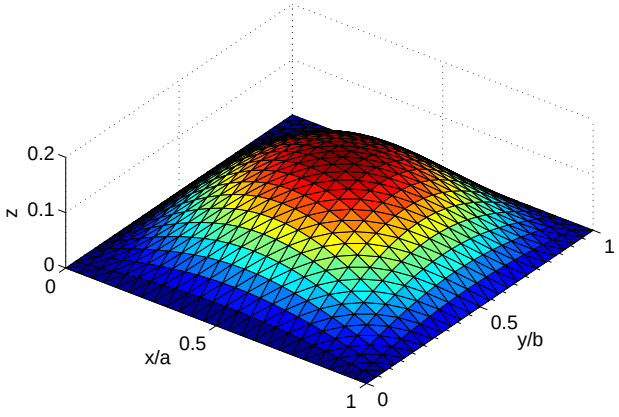

(a) Mode 1 ($\bar{\omega}$=1.6674)

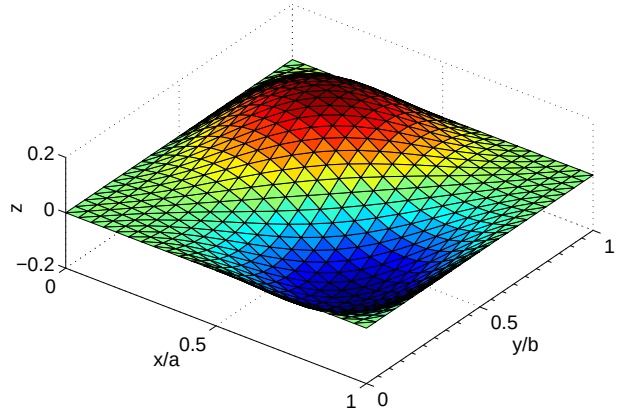

(b) Mode 2 ($\bar{\omega}$=3.9923)

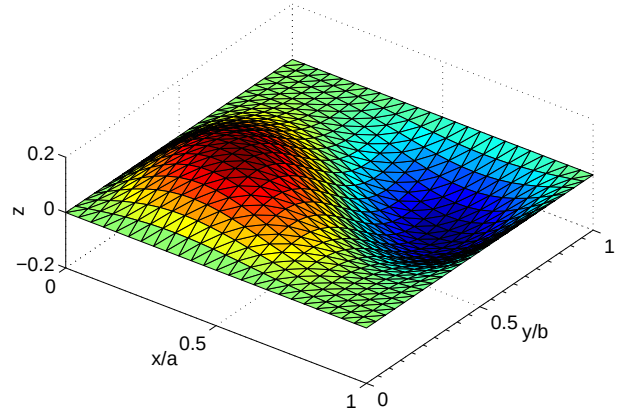

(c) Mode 3 ($\bar{\omega}$=4.0021)

Figure 5: First three shape modes of Al^*/ZrO_2 simply supported square plates (a/h=10, p=1, Type A).

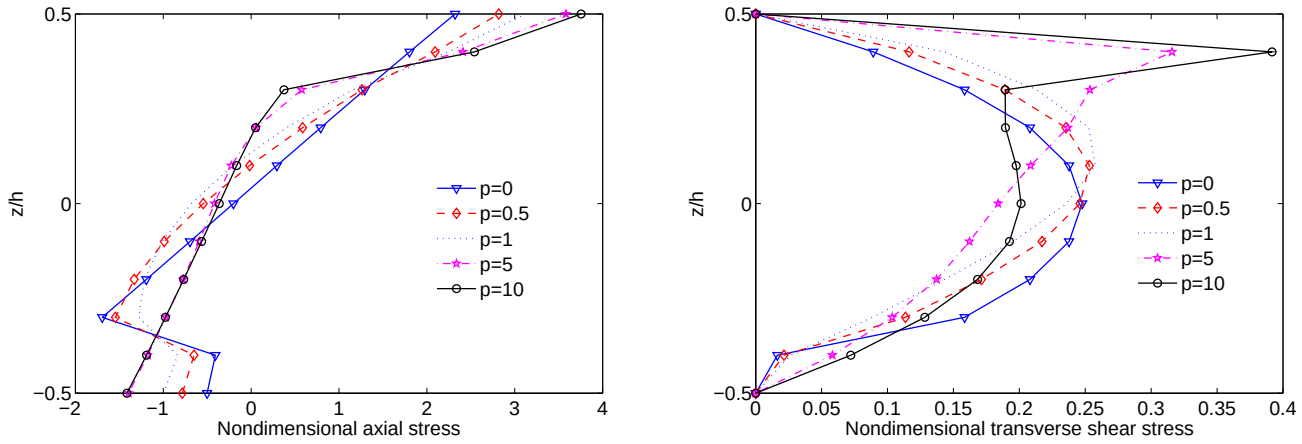

(a) $\bar{\sigma}_{xx}$ (1-2-1 Al/Al_2O_3 plate)

(b) $\bar{\sigma}_{xz}$ (1-2-1 Al/Al_2O_3 plate)

Figure 6: Nondimensional membrane stress $\bar{\sigma}_{xx}$ and transverse shear stress $\bar{\sigma}_{xz}$ through the thickness direction of Al/Al_2O_3 simply supported square plates subjected to sinusoidal load (a/h=10, Type B).

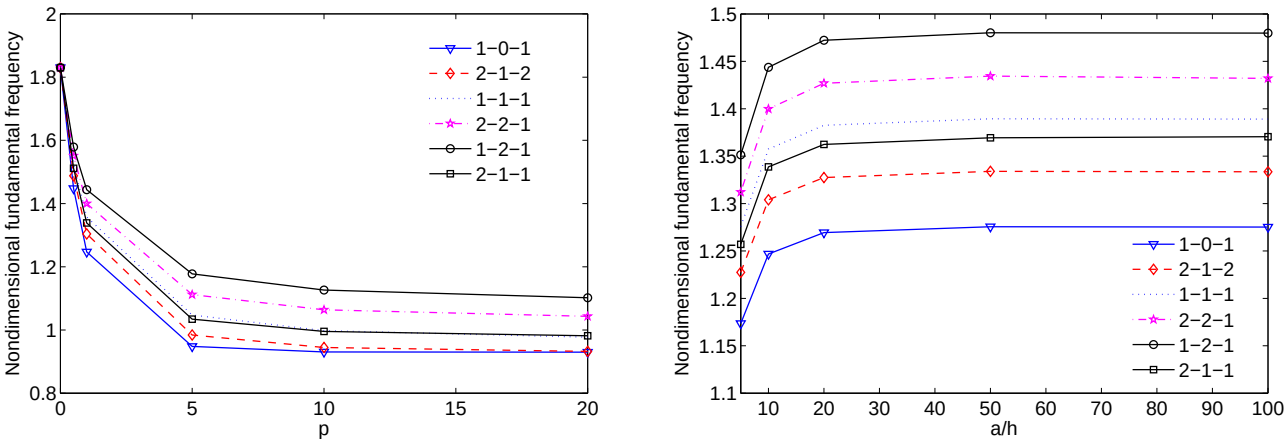

(a) a/h=10 (b) p=1

Figure 7: Effect of the power-law index p and side-to-thickness ratio on the nondimensional fundamental frequency ($\hat{\omega}$) of Al/Al_2O_3 simply supported square plates (Type C).